International Journal of Mechanical Engineering Research And Development (IJMERD)

ISSN 2248 – 9347(Print)
ISSN 2248 – 9355(Online),
Volume 5, Number 1, January – April (2015), pp. 01-17

IJMERD

© PRJ PUBLICATION

AİR TRANSİENT COOLİNG CHARACTERİSTİCS İN THE ENTRY REGİONS OF DUCTS: AN EXTENSİON TO NON-CİRCULAR DUCT GEOMETRY

MURAT TEKELİOĞLU

Department of Mechanical Engineering, Karabük University,
Karabük, Turkey

ABSTRACT

The cross-section duct geometry relates differently to the rate of heat transfer. The purpose of this paper is to investigate the air cooling characteristics on the triangular, rectangular, circular, and square cross-section ducts. In the work, the entry region was studied and the transient solutions were presented. The thermally and hydrodynamically-developing flow condition (combined entry) was considered with its appropriate expressions. As the result, the transient-thermal solutions were obtained in the combined entry region. Identical flow cross-section areas were considered on the ducts. Air was the flowing medium but other fluids could also be substituted. Required pump power was given comparatively on each duct. The triangular cross-section duct was seen to enhance the heat transfer most. The results of this study will shed light as to what type of the duct geometry will provide the most effective air cooling. The results establish the first fundamentals with air without the need to perform simulations on the simulation softwares. From a more specific point, the findings of this paper will be important to the design studies of such ducts before their manufacture.

Keywords: Transient solution, Combined entry, Air cooling, Triangular duct, Rectangular duct, Circular duct, Square duct

1. INTRODUCTİON

Heat transfer studies were performed with various fluids: A macro channel of $20mm$ nominal diameter and $30mm$ of length was considered with water to predict the heat removal from micro-size channels after placement of an insert into the channel (Kong and Ooi, 2013). In their work, $1mm$ and $300\mu m$ gap sizes and a Reynolds number range between $1{,}000$ and $5{,}500$ was studied numerically and experimentally. Another experimental study was conducted on the combined heat transfer (free convection + forced convection) problem for hydrodynamically fully-developed and thermally-developing laminar air flow under constant heat flux condition (Mohammed and Salman, 2007). A refined expression of the convective

heat transfer coefficient on the simultaneously developing hydrodynamic and thermal entrance regions of a circular pipe was presented from a numerical solution (Nguyen, 1993). The author there numerically investigated the constant temperature and constant heat flux cases on the laminar-flow Newtonian fluids. The turbulent mixing length theory was extrapolated down to the laminar region to present the average heat transfer coefficients in the short entry region of a tube (Sarma *et al.*, 2004). A three-dimensional numerical simulation was implemented on micro-channel heat sinks (Chen *et al.*, 2009). In their work, trough type (that is, open top) triangular, rectangular, and trapezodial silicon micro channel heat sinks were studied. Turbulence at the combined entry was experimentally studied (Kays and Crawford, 1993) and a figure representing the Nu_x/Nu_∞ curves were given for various entry conditions: abrupt-contraction, 90° right-angle bend, 180° round bend, and normal entry. Their figure was given under $Re_{Dh} \cong 50{,}000$.

In applications where relatively high-temperature (hot) air is discharged, it is of concern to select the most appropriate duct geometry. Because of different cooling characteristics of different cross-section ducts, a decision is required to be made as to which cross-section duct to choose. In this respect, an entry region study is a more involved picture and gives details of the heat transfer process. It is of interest to know the temperature behavior at the combined entry region thereby to choose the suitable duct geometry. Fully-developed hydrodynamic and thermal regions are well studied in the literature. This paper aims to determine the air cooling characteristics of different cross-section ducts where the air properties are temperature-dependent. Air transient thermal cooling solutions were included for each duct type in the combined entry region.

2. CORRELATİONS

In the study, hydrodynamic entrance length ($x_{fd,h}(T_m)$) and thermal entrance length ($x_{fd,t}(T_m)$) were calculated (Bergman *et al.*, 2011) of each duct type, respectively, from $x_{fd,h}(T_m) \approx 0.05 \cdot D_h \cdot Re_{Dh}(T_m)andx_{fd,t}(T_m) \approx x_{fd,h}(T_m) \cdot \Pr(T_m)$. Here, D_h is the hydraulic diameter, $Re_{Dh}(T_m)$ is the Reynolds number based on D_h, and $\Pr(T_m)$ is the Prandtl number (Bergman *et al.*, 2011). In these, D_h was defined as $D_h = (4 \cdot A_c)/P$ where A_c is the flow cross-section area and P is the flow wetted perimeter. In the calculations of $Re_{Dh}(T_m)$ and $\Pr(T_m)$, the air properties were evaluated at $T_m = (T_{in} + T_{out})/2$.

Table 1 includes the list of the calculated $x_{fd,h}(T_m)$ and $x_{fd,t}(T_m)$ values on each duct type. Each duct type analyzed maintained a fractional combined entry as the result of the calculated values of $x_{fd,h}(T_m)$ and $x_{fd,t}(T_m)$.

In the thermally-developing and hydrodynamically fully developed region ($T_s = cst$), an expression for the average Nusselt number ($\overline{Nu}_{Dh}(T_m)$) was included (Bergman *et al.*, 2011)

$$\overline{Nu}_{Dh}(T_m) = 3.66 + \frac{0.0668 \cdot Gz_{Dh}(T_m)}{1 + 0.04 \cdot Gz_{Dh}^{\frac{2}{3}}(T_m)} \quad (1)$$

where$Gz_{Dh}(T_m) = \left(\frac{D_h}{x}\right) Re_{Dh}(T_m)\Pr(T_m)$ and $x \le x_{fd,t}$ and $x > x_{fd,h}$. In the both thermally and hydrodynamically fully-developed region ($T_s = cst$), Nusselt number (Nu_{Dh}) was given $Nu_{Dh} = 3.66$(Bergman *et al.*, 2011). There are several correlations available ($T_s = cst$) in the combined entry region, e.g., (Bergman *et al.*, 2011)

$$\bar{h}_{Air}(T_m) = \left[\frac{\frac{3.66}{tanh\left[2.264 \cdot Gz_{Dh}^{-\frac{1}{3}}(T_m) + 1.7 \cdot Gz_{Dh}^{-\frac{2}{3}}(T_m)\right]} + 0.0499 \cdot Gz_{Dh}(T_m) \cdot tanh\left[Gz_{Dh}^{-1}(T_m)\right]}{tanh\left[2.432 \cdot Pr^{\frac{1}{6}}(T_m) \cdot Gz_{Dh}^{-\frac{1}{6}}(T_m)\right]} \right] \cdot \frac{k_{Air}(T_m)}{D_h} \quad (2)$$

which is valid for $Pr \gtrsim 0.1$. Equation (2) is recommended as long as the flow is both thermally and hydrodynamically developing. In the combined entry region, it was alternatively recommended (Sieder and Tate, 1936)

$$\overline{Nu}_{Dh}(T_m) = 1.86 \cdot \left(\frac{Re_{Dh}(T_m) \cdot \mathrm{Pr}\,(T_m) \cdot D_h}{L}\right) \cdot \left(\frac{\mu_b(T_m)}{\mu_s(T_m)}\right)^{0.4} \quad (3)$$

which is valid for $Pr > 0.5$ in which all properties are evaluated at T_m except μ_s which is evaluated at T_s. Equation (3)is a little bit less resorted to, therefore, wherever possible, the correlation of Eq. (2) is recommended in the combined entry region. Also, the correlations of Eqs. (2) and (3) represent the average convective heat transfer coefficients. Therefore, a local convective heat transfer coefficient (h_x) needs to be substituted for a better heat transfer analysis in the combined entry region.

In the analysis, the flow condition (as determined from the calculated values of $x_{fd,h}(T_m)$ and $x_{fd,t}(T_m)$ seen in Table 1) inside the ducts was both thermally and hydrodynamically-developing. In the combined entry region, local Nusselt number (Nu_x) values ($T_s = cst$) were taken from Kays and Crawford (1993). Correspondingh_x values were calculated from the Nu_x values. Table 2 includes the Nu_x values.

Table 1$x_{fd,h}(T_m)$ and $x_{fd,t}(T_m)$ values

cross-section	$x_{fd,h}(T_m)^1$ $[m]$	$x_{fd,t}(T_m)^2$ $[m]$	$Re_{Dh}(T_m)^1$ $[-]$
$\dot{m}_{Air} = 0.036kg/h$			
triangular	0.027	0.018	125.8
rectangular	0.026	0.018	88.29
circular	0.026	0.018	76.311
square	0.026	0.018	86.457
$\dot{m}_{Air} = 0.18kg/h$			
triangular	0.13	0.09	613.66
rectangular	0.126	0.087	418.929
circular	0.124	0.085	357.744
square	0.126	0.087	410.06
$\dot{m}_{Air} = 0.36kg/h$			
triangular	0.254	0.175	1,200.1
rectangular	0.244	0.168	813.355
circular	0.24	0.165	694.076
square	0.243	0.168	794.922
$\dot{m}_{Air} = 0.72kg/h$			
triangular	0.495	0.341	2,337.99
rectangular	0.474	0.327	1,581
circular	0.467	0.321	1,350
square	0.473	0.326	1,546

[1]$Re_{Dh}(T_m)$ and [2] $Re_{Dh}(T_m)$ and Pr (T_m) calculated at T_m, $T_m = \frac{T_{in}+T_{out}}{2} = \frac{(250+273.15)K+T_6}{2}$.$T_6$ was found from the solution (See the section Analysis).

Table 2 Nu_x with x^+

$x^+ = \frac{x/r_0}{RePr}$ [−]	Nu_x[1] $(Pr = 0.7)$ [−]
0.001	16.8
0.002	12.6
0.004	9.6
0.006	8.25
0.01	6.8
0.02	5.3
0.05	4.2
100 (∞)	3.66

[1] $Nu_x = \frac{h_x D_h}{k_{Air}}$.

3. ANALYSIS

Triangular, rectangular, circular, and square duct dimensions were shown in Fig. 1. Figure 2 illustrates the twelve-node arrangement taken on each duct geometry. h_x values calculated of Table 2 decreased in the combined entry region finally settling on to the value $h_x = (3.66 \cdot k_{Air}/D_h)$in the hydrodynamically and thermally fully-developed region. In the postulation of the heat transfer equation, the air axial heat conduction was included. The axial heat conduction contribution becomes even more important in the analyses concerning thermally more conductive fluids such as water. However, the thermal conductivity of air is bad in comparison to that of water. As Nu decreases (16.8 to 3.66), air thermal conductivity contribution in the heat transfer process increases and the effect was considered in the heat transfer equations. Heat transfer equations were written on each of the twelve nodal points. Temperature-dependent properties were indicated with the parentheses and square brackets beside properties: $k_{Air}[\dots]$ and $c_{p,Air}[\dots]$ terms indicate, respectively, the temperature-dependent thermal conductivity and specific heat values of air. Since the temperature-dependent properties were used in the transient (time-dependent) solution, a spreadsheet solution with Excel, for example, is difficult in the current problem.

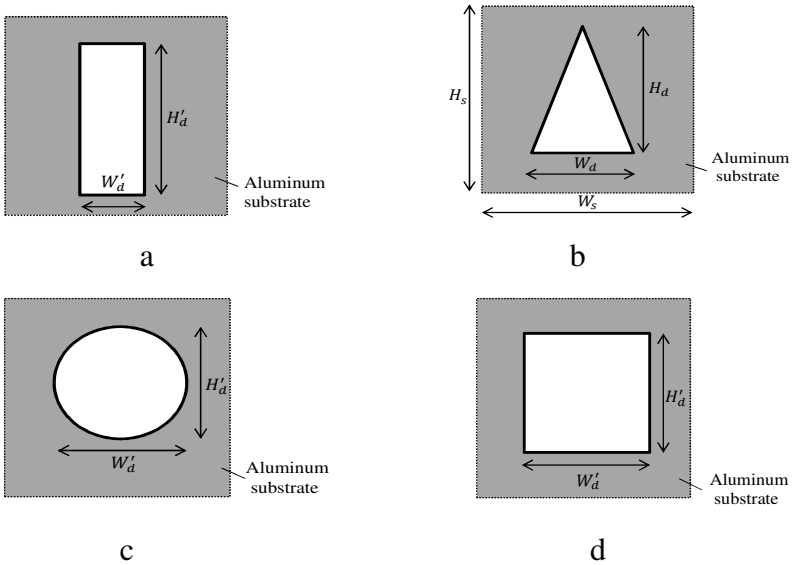

Figure 1. Frontal views of the duct types. W_s represents the width and H_s represents the height of the aluminum substrate ($W_s = H_s = 25 \cdot 10^{-3}m$). Identical flow cross-section areas ($A_f = 3.75 \cdot 10^{-5}m^2$) were considered on the ducts. a) $W_d = 5 \cdot 10^{-3}m$, $H_d = 15 \cdot 10^{-3}m$ (triangular cross-section). b) $W'_d = 5 \cdot 10^{-3}m$, $H'_d = 7.5 \cdot 10^{-3}m$ (rectangular cross section). c) $W'_d = H'_d = 6.91 \cdot 10^{-3}m$ (circular cross-section). d) $W'_d = H'_d = 6.124 \cdot 10^{-3}m$ (square cross-section).

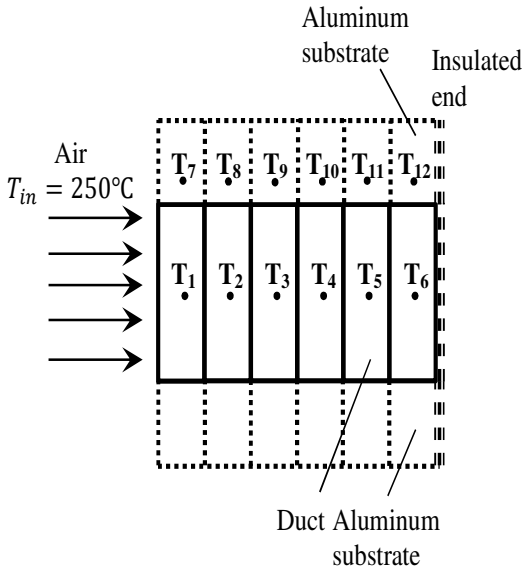

Figure 2. Nodal arrangement. Conductive heat transfer of the aluminum substrate, conductive heat transfer of the air, mass flow (enthalpy) of the air, and convective heat transfer of the air were considered.

Air:
Node 1:

$$\frac{\mathrm{D}T_1}{\mathrm{d}t} = \frac{\left\{\begin{array}{c} \dot{m}_{Air}\cdot c_{p,Air}\left[\frac{T_{in}+T_1}{2}\right]\cdot(T_{in}-T_1)+ \\ \dot{m}_{Air}\cdot c_{p,Air}\left[\frac{T_2+T_1}{2}\right]\cdot(T_2-T_1)+ \\ k_{Air}\left[\frac{T_{in}+T_1}{2}\right]\cdot A_c\cdot\frac{(T_{in}-T_1)}{\Delta x}+ \\ k_{Air}\left[\frac{T_2+T_1}{2}\right]\cdot A_c\cdot\frac{(T_2-T_1)}{\Delta x}+ \\ \left(\frac{\int_0^{\Delta x} Nu_{Air}(x,T_1)dx}{\Delta x}\cdot\frac{k_{Air}(T_1)}{D_h}\right)\cdot A_{lat}\cdot(T_7-T_1) \end{array}\right\}}{\rho_{Air}(T_1)\cdot V_{Air}\cdot c_{p,Air}(T_1)} \quad (4)$$

Node 2:

$$\frac{\mathrm{D}T_2}{\mathrm{d}t} = \frac{\left\{\begin{array}{c} \dot{m}_{Air}\cdot c_{p,Air}\left[\frac{T_1+T_2}{2}\right]\cdot(T_1-T_2)+ \\ \dot{m}_{Air}\cdot c_{p,Air}\left[\frac{T_3+T_2}{2}\right]\cdot(T_3-T_2)+ \\ k_{Air}\left[\frac{T_1+T_2}{2}\right]\cdot A_c\cdot\frac{(T_1-T_2)}{\Delta x}+ \\ k_{Air}\left[\frac{T_3+T_2}{2}\right]\cdot A_c\cdot\frac{(T_3-T_2)}{\Delta x}+ \\ \left(\frac{\int_{\Delta x}^{2\cdot\Delta x} Nu_{Air}(x,T_2)dx}{\Delta x}\cdot\frac{k_{Air}(T_2)}{D_h}\right)\cdot A_{lat}\cdot(T_8-T_2) \end{array}\right\}}{\rho_{Air}(T_2)\cdot V_{Air}\cdot c_{p,Air}(T_2)} \quad (5)$$

Node 3:

$$\frac{\mathrm{D}T_3}{\mathrm{d}t} = \frac{\left\{\begin{array}{c} \dot{m}_{Air}\cdot c_{p,Air}\left[\frac{T_2+T_3}{2}\right]\cdot(T_2-T_3)+ \\ \dot{m}_{Air}\cdot c_{p,Air}\left[\frac{T_4+T_3}{2}\right]\cdot(T_4-T_3)+ \\ k_{Air}\left[\frac{T_2+T_3}{2}\right]\cdot A_c\cdot\frac{(T_2-T_3)}{\Delta x}+ \\ k_{Air}\left[\frac{T_4+T_3}{2}\right]\cdot A_c\cdot\frac{(T_4-T_3)}{\Delta x}+ \\ \left(\frac{\int_{2\cdot\Delta x}^{3\cdot\Delta x} Nu_{Air}(x,T_3)dx}{\Delta x}\cdot\frac{k_{Air}(T_3)}{D_h}\right)\cdot A_{lat}\cdot(T_9-T_3) \end{array}\right\}}{\rho_{Air}(T_3)\cdot V_{Air}\cdot c_{p,Air}(T_3)} \tag{6}$$

Node 4:

$$\frac{\mathrm{D}T_4}{\mathrm{d}t} = \frac{\left\{\begin{array}{c} \dot{m}_{Air}\cdot c_{p,Air}\left[\frac{T_3+T_4}{2}\right]\cdot(T_3-T_4)+ \\ \dot{m}_{Air}\cdot c_{p,Air}\left[\frac{T_5+T_4}{2}\right]\cdot(T_5-T_4)+ \\ k_{Air}\left[\frac{T_3+T_4}{2}\right]\cdot A_c\cdot\frac{(T_3-T_4)}{\Delta x}+ \\ k_{Air}\left[\frac{T_5+T_4}{2}\right]\cdot A_c\cdot\frac{(T_5-T_4)}{\Delta x}+ \\ \left(\frac{\int_{3\cdot\Delta x}^{4\cdot\Delta x} Nu_{Air}(x,T_4)dx}{\Delta x}\cdot\frac{k_{Air}(T_4)}{D_h}\right)\cdot A_{lat}\cdot(T_{10}-T_4) \end{array}\right\}}{\rho_{Air}(T_4)\cdot V_{Air}\cdot c_{p,Air}(T_4)} \tag{7}$$

Node 5:

$$\frac{\mathrm{D}T_5}{\mathrm{d}t} = \frac{\left\{\begin{array}{c} \dot{m}_{Air}\cdot c_{p,Air}\left[\frac{T_4+T_5}{2}\right]\cdot(T_4-T_5)+ \\ \dot{m}_{Air}\cdot c_{p,Air}\left[\frac{T_6+T_5}{2}\right]\cdot(T_6-T_5)+ \\ k_{Air}\left[\frac{T_4+T_5}{2}\right]\cdot A_c\cdot\frac{(T_4-T_5)}{\Delta x}+ \\ k_{Air}\left[\frac{T_6+T_5}{2}\right]\cdot A_c\cdot\frac{(T_6-T_5)}{\Delta x}+ \\ \left(\frac{\int_{4\cdot\Delta x}^{5\cdot\Delta x} Nu_{Air}(x,T_5)dx}{\Delta x}\cdot\frac{k_{Air}(T_5)}{D_h}\right)\cdot A_{lat}\cdot(T_{11}-T_5) \end{array}\right\}}{\rho_{Air}(T_5)\cdot V_{Air}\cdot c_{p,Air}(T_5)} \tag{8}$$

Node 6:

$$\frac{\mathrm{D}T_6}{\mathrm{d}t} = \frac{\left\{\begin{array}{c} \dot{m}_{Air}\cdot c_{p,Air}\left[\frac{T_5+T_6}{2}\right]\cdot(T_5-T_6)+ \\ k_{Air}\left[\frac{T_5+T_6}{2}\right]\cdot A_c\cdot\frac{(T_5-T_6)}{\Delta x}+ \\ \left(\frac{\int_{5\cdot\Delta x}^{6\cdot\Delta x} Nu_{Air}(x,T_6)dx}{\Delta x}\cdot\frac{k_{Air}(T_6)}{D_h}\right)\cdot A_{lat}\cdot(T_{12}-T_6) \end{array}\right\}}{\rho_{Air}(T_6)\cdot V_{Air}\cdot c_{p,Air}(T_6)} \tag{9}$$

Aluminum substrate:

Node 7:

$$\frac{\mathrm{D}T_7}{\mathrm{d}t} = \frac{\left\{\begin{array}{c} k_{Al}\left[\frac{T_8+T_7}{2}\right]\cdot A_{Al}\cdot\frac{(T_8-T_7)}{\Delta x}+ \\ \left(\frac{\int_0^{\Delta x} Nu_{Air}(x,T_1)dx}{\Delta x}\cdot\frac{k_{Air}(T_1)}{D_h}\right)\cdot A_{lat}\cdot(T_1-T_7) \end{array}\right\}}{\rho_{Al}(T_7)\cdot V_{Al}\cdot c_{p,Al}(T_7)} \tag{10}$$

Node 8:

$$\frac{\mathrm{D}T_8}{\mathrm{d}t} = \frac{\left\{\begin{array}{c} k_{Al}\left[\frac{T_7+T_8}{2}\right]\cdot A_{Al}\cdot\frac{(T_7-T_8)}{\Delta x}+ \\ k_{Al}\left[\frac{T_9+T_8}{2}\right]\cdot A_{Al}\cdot\frac{(T_9-T_8)}{\Delta x}+ \\ \left(\frac{\int_{\Delta x}^{2\cdot\Delta x} Nu_{Air}(x,T_2)dx}{\Delta x}\cdot\frac{k_{Air}(T_2)}{D_h}\right)\cdot A_{lat}\cdot(T_2-T_8) \end{array}\right\}}{\rho_{Al}(T_8)\cdot V_{Al}\cdot c_{p,Al}(T_8)} \tag{11}$$

Node 9:

$$\frac{\mathrm{D}T_9}{\mathrm{d}t} = \frac{\left\{\begin{array}{c} k_{Al}\left[\frac{T_8+T_9}{2}\right]\cdot A_{Al}\cdot\frac{(T_8-T_9)}{\Delta x}+ \\ k_{Al}\left[\frac{T_{10}+T_9}{2}\right]\cdot A_{Al}\cdot\frac{(T_{10}-T_9)}{\Delta x}+ \\ \left(\frac{\int_{2\cdot\Delta x}^{3\cdot\Delta x} Nu_{Air}(x,T_3)dx}{\Delta x}\cdot\frac{k_{Air}(T_3)}{D_h}\right)\cdot A_{lat}\cdot(T_3-T_9) \end{array}\right\}}{\rho_{Al}(T_9)\cdot V_{Al}\cdot c_{p,Al}(T_9)} \tag{12}$$

Node 10:

$$\frac{\mathrm{D}T_{10}}{\mathrm{d}t} = \frac{\left\{\begin{array}{c} k_{Al}\left[\frac{T_9+T_{10}}{2}\right]\cdot A_{Al}\cdot\frac{(T_9-T_{10})}{\Delta x}+ \\ k_{Al}\left[\frac{T_{11}+T_{10}}{2}\right]\cdot A_{Al}\cdot\frac{(T_{11}-T_{10})}{\Delta x}+ \\ \left(\frac{\int_{3\cdot\Delta x}^{4\cdot\Delta x} Nu_{Air}(x,T_4)dx}{\Delta x}\cdot\frac{k_{Air}(T_4)}{D_h}\right)\cdot A_{lat}\cdot(T_4-T_{10}) \end{array}\right\}}{\rho_{Al}(T_{10})\cdot V_{Al}\cdot c_{p,Al}(T_{10})} \tag{13}$$

Node 11:

$$\frac{\mathrm{D}T_{11}}{\mathrm{d}t} = \frac{\left\{\begin{array}{c} k_{Al}\left[\frac{T_{10}+T_{11}}{2}\right]\cdot A_{Al}\cdot\frac{(T_{10}-T_{11})}{\Delta x}+ \\ k_{Al}\left[\frac{T_{12}+T_{11}}{2}\right]\cdot A_{Al}\cdot\frac{(T_{12}-T_{11})}{\Delta x}+ \\ \left(\frac{\int_{4\cdot\Delta x}^{5\cdot\Delta x} Nu_{Air}(x,T_5)dx}{\Delta x}\cdot\frac{k_{Air}(T_5)}{D_h}\right)\cdot A_{lat}\cdot(T_5-T_{11}) \end{array}\right\}}{\rho_{Al}(T_{11})\cdot V_{Al}\cdot c_{p,Al}(T_{11})} \tag{14}$$

Node 12:

$$\frac{\mathrm{D}T_{12}}{\mathrm{d}t} = \frac{\left\{ \begin{array}{c} k_{Al}\left[\frac{T_{11}+T_{12}}{2}\right]\cdot A_{Al}\cdot\frac{(T_{11}-T_{12})}{\Delta x} + \\ \left(\frac{\int_{5\cdot\Delta x}^{6\cdot\Delta x} Nu_{Air}(x,T_6)dx}{\Delta x}\cdot\frac{k_{Air}(T_6)}{D_h}\right)\cdot A_{lat}\cdot(T_6-T_{12}) \end{array} \right\}}{\rho_{Al}(T_{12})\cdot V_{Al}\cdot c_{p,Al}(T_{12})} \tag{15}$$

In order to solve the system of equations represented by Eqs. (4-15), the insulated-end boundary condition was imposed and the equations were solved simultaneously. Adaptive-step ode solver (rkadapt) was used (with $1{,}000$ points) on MathCAD.

For nodes $(1-6)$ (air), the local convective heat transfer coefficients, $\bar{h}_x(T_i) = \left(\int_{\Delta x_i}^{\Delta x_{i+1}} Nu_{Air}(x,T_i)dx\right)/\Delta x \cdot (k_{Air}(T_i)/D_h)$ $(i=1,n;\ n=6)$ were calculated from the values in Table 2. The so-obtained $\bar{h}_x(T_i)$ values were substituted in the equations. $\bar{h}_x(T_i)$ valueswere linearly interpolated in the combined entry region over seven data points of Table 2.

Throughout temperature-dependent properties of the aluminum substrate and air were used. The properties were taken from Bergman *et al.* (2011). The parameters were $\Delta x = 10mm$, $T_{in} = (250+273.15)K$, and the entire system was at $300K$ initially.

4. RESULTS

4.1. Air Cooling Effect

The analysis results for the triangular, rectangular, circular, and square cross-section geometry ducts ($\dot{m}_{Air} = 0.036kg/h$) were shown in Figs. (3-6), in Figs. (7-10) ($\dot{m}_{Air} = 0.18kg/h$), in Figs.(11-14) ($\dot{m}_{Air} = 0.36kg/h$), and in Figs.(15-18) ($\dot{m}_{Air} = 0.72kg/h$).

The calculated exit temperatures (T_6) for the triangular, rectangular, circular, and square-cross-section ducts were, respectively, $300.97K$, $304.9K$, $308.06K$, and $305.29K$ ($\dot{m}_{Air} = 0.036kg/h$), $318.07K$, $343.45K$, $357.19K$, and $344.24K$ ($\dot{m}_{Air} = 0.18kg/h$), $334.75K$, $368.48K$, $384.53K$, and $370.73K$ ($\dot{m}_{Air} = 0.36kg$), $355.91K$, $395.22K$, $412.7K$, and $397.7K$ ($\dot{m}_{Air} = 0.72kg/h$). Note that $x_{fd,h}(T_m)$ and $x_{fd,t}(T_m)$ values listed in Table 1 are to be evaluated withthese temperatures. The case with $\dot{m}_{Air} = 0.036kg/h$ involves a few nodes (nodes 1 and 2 for $x_{fd,h}$ and solely node 1 for $x_{fd,t}$) in this respect. Hence, in terms of the effect of cooling, triangular cross-section duct was preferable which was followed by the rectangular, square, and circular-cross-section ducts. As $\dot{m}_{Air}$ was increased, the simulation time was observed to be also increasing when calculating the aluminum substrate temperatures (nodes 7-12). Aluminum substrate temperature calculation run times were about $10min$ at $t = 60s$ of calculation time for $\dot{m}_{Air} = 0.72kg/h$. In the results, it was observed that the aluminum substrate temperature did not show a quick response but reaching a steady-state temperature after some time. The aluminum substrate temperature increased slowly relative to the air. The aluminum substrate nodal temperatures eventually stabilized and reached their steady-state values. The reason for the slow increase of the aluminum substrate temperature was because of the large "thermal mass (C)" of the aluminum substrate which is defined as $C = m \cdot c_p$ where m is the mass (kg) and c_p is the specific heat at constant pressure ($J/(kg \cdot K)$). In the present analysis, the thermal mass of the aluminum substrate was about $4.656 \cdot 10^4$ times greater compared to that of air at $T_m = [(250+273.15)K + T_6(=300.97K)]/2 = 412.06K$ for the triangular duct ($\dot{m}_{Air} = 0.036kg/h$). Such high level

of the aluminum substrate thermal mass makes aluminum a perfect heat sink allowing it to absorb large amounts of heat from the surrounding air. An increase of the volume of the aluminum substrate (with both W_s and H_s or either of $W_s$or H_s) further increases the thermal mass of the aluminum substrate relative to that of air. Even after taking identical air and aluminum substrate volumes, thermal mass of the aluminum substrate is $2.972 \cdot 10^3$ times greater compared to that of air.

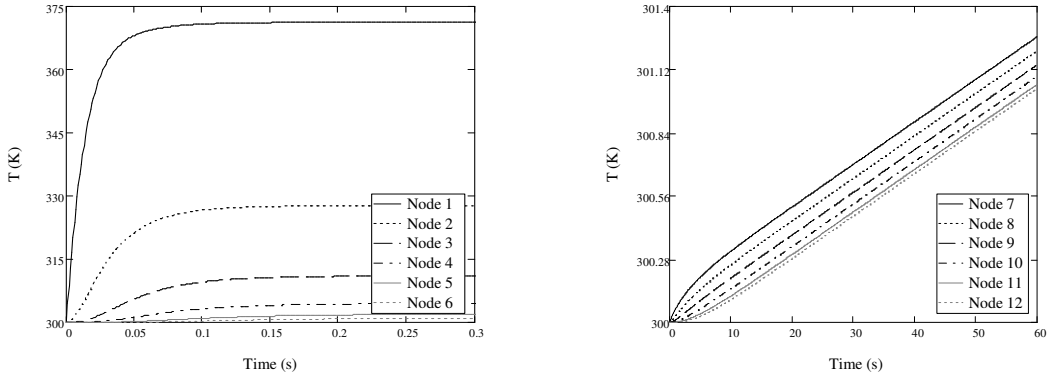

(a) (b)

Figure 3. Cooling characteristics of the triangular channel ($\dot{m}_{Air} = 0.036kg/h$): a) Air, b) Aluminum substrate.

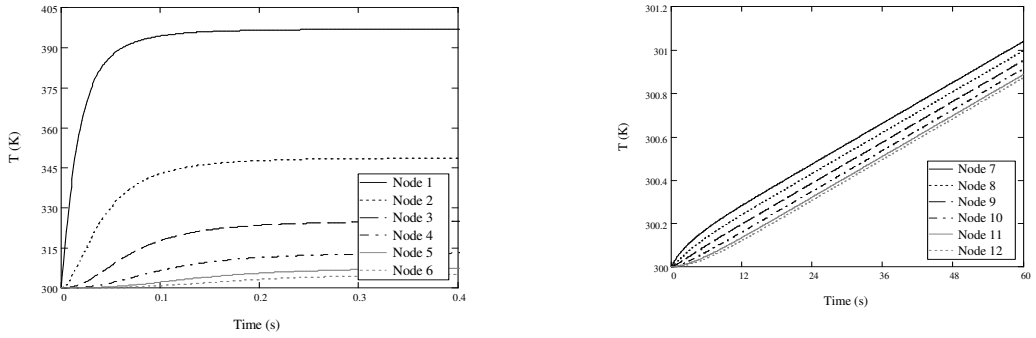

(a) **(b)**

Figure 4. Cooling characteristics of the rectangular duct (m˙_Air=0.036kg/h): a) Air, b) Aluminum substrate

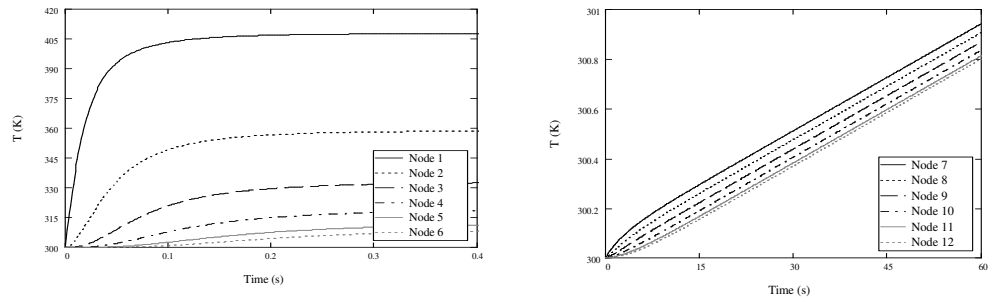

(a) **(b)**

Figure 5. Cooling characteristics of the circular duct (m˙_Air=0.036kg/h): a) Air, b) Aluminum substrate.

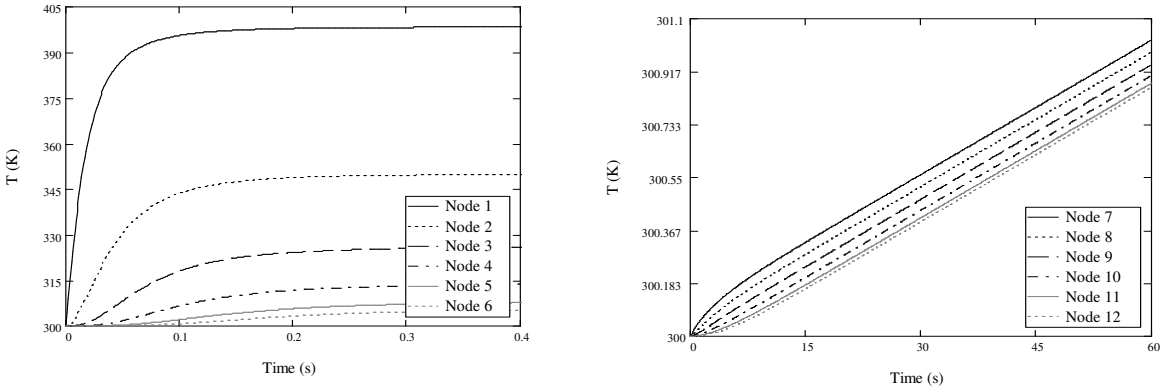

(a) **(b)**

Figure 6. Cooling characteristics of the square duct (m ̇_Air=0.036kg/h): a) Air, b) Aluminum substrate.

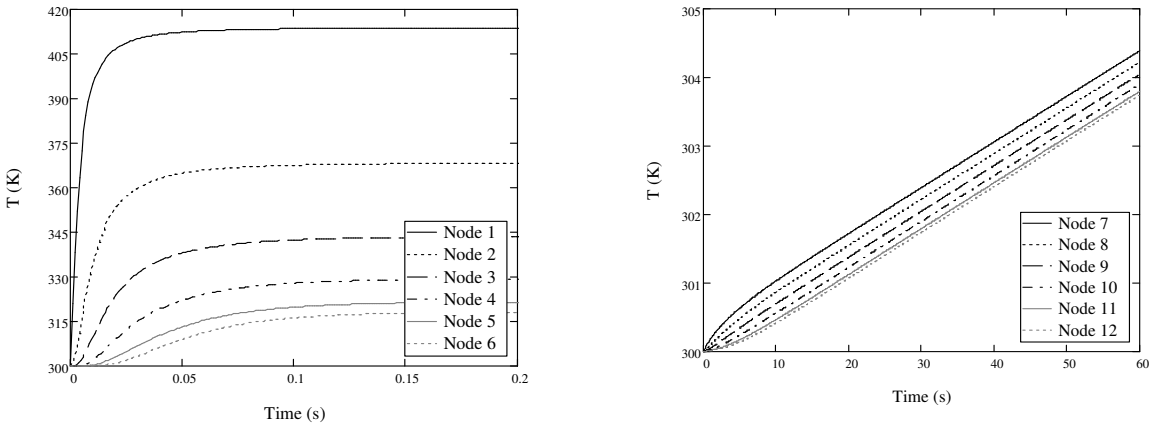

(a) (b)

Figure 7. Cooling characteristics of the triangular channel (m ̇_Air=0.18kg/h): a) Air, b) Aluminum substrate.

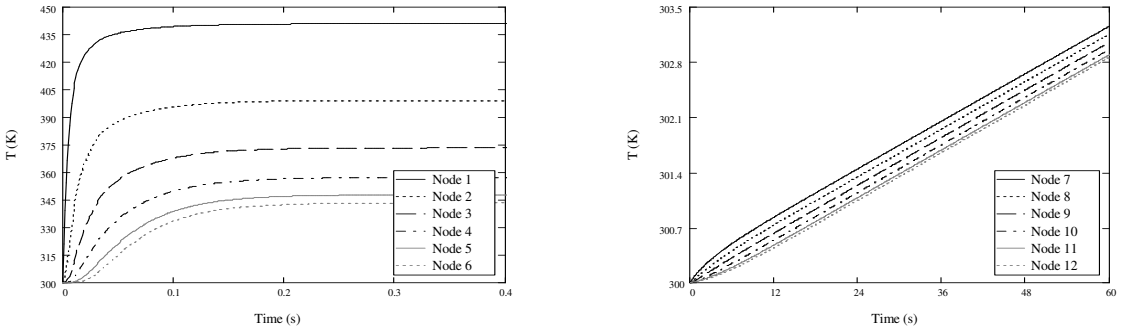

(a) **(b)**

Figure 8. Cooling characteristics of the rectangular duct (m ̇_Air=0.18kg/h): a) Air, b) Aluminum substrate.

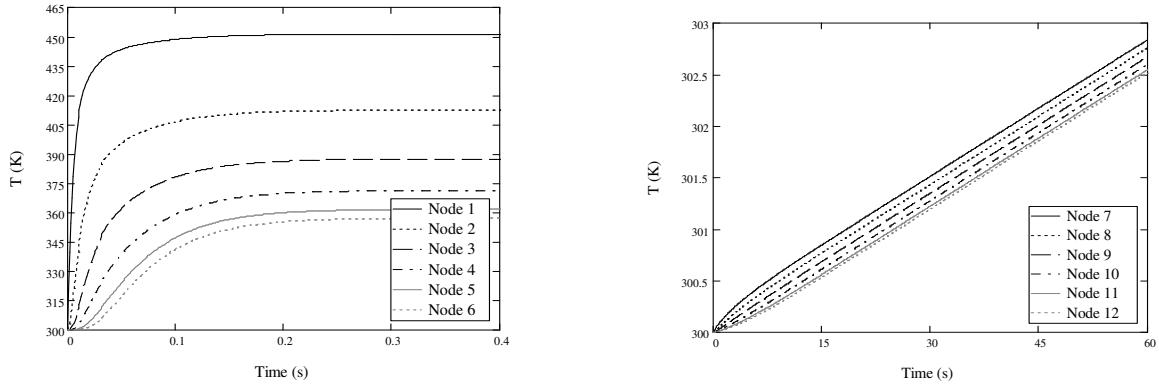

(a) **(b)**

Figure 9. Cooling characteristics of the circular duct ($\dot{m}_{Air} = 0.18kg/h$): a) Air, b) Aluminum substrate.

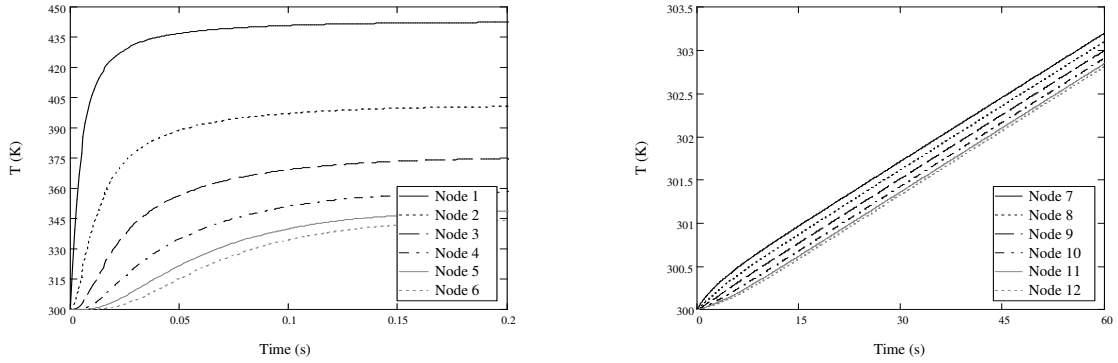

(a) **(b)**

Figure 10. Cooling characteristics of the square duct ($\dot{m}_{Air} = 0.18kg/h$): a) Air, b) Aluminum substrate.

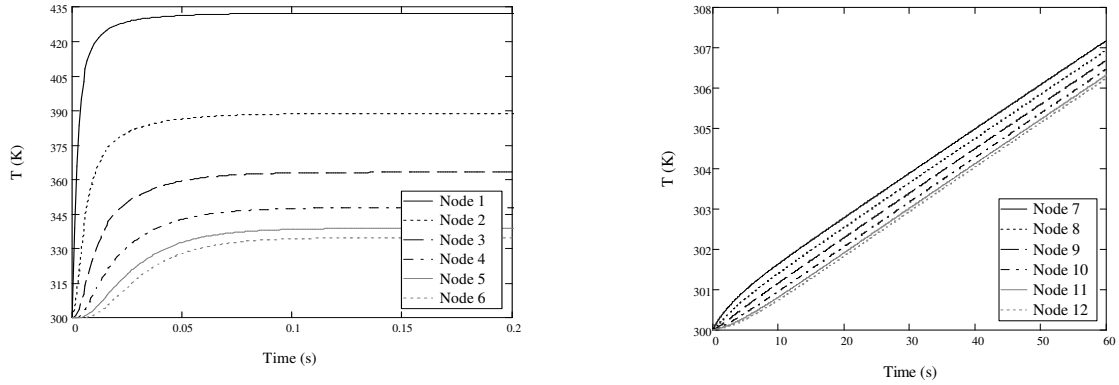

(a) **(b)**

Figure 11. Cooling characteristics of the triangular channel ($\dot{m}_{Air} = 0.36kg/h$): a) Air, b) Aluminum substrate.

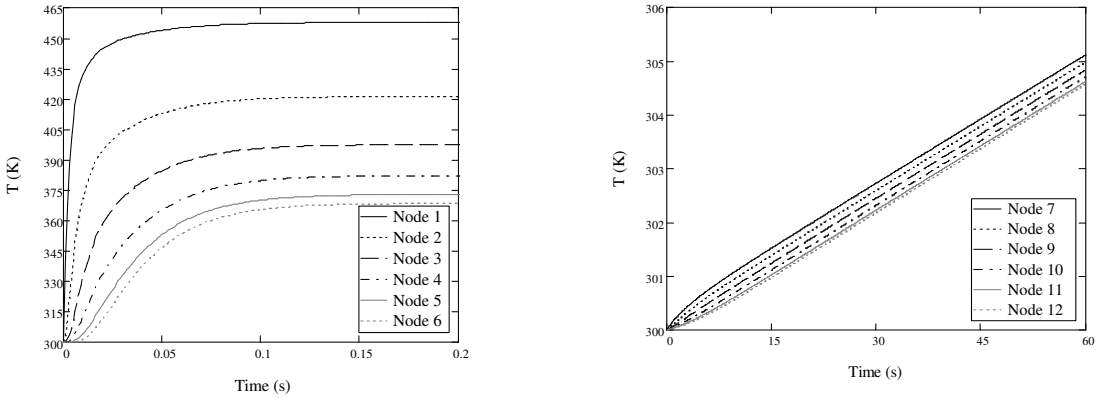

(a) **(b)**

Figure 12. Cooling characteristics of the rectangular duct ($\dot{m}_{Air} = 0.36kg/h$): a) Air, b) Aluminum substrate.

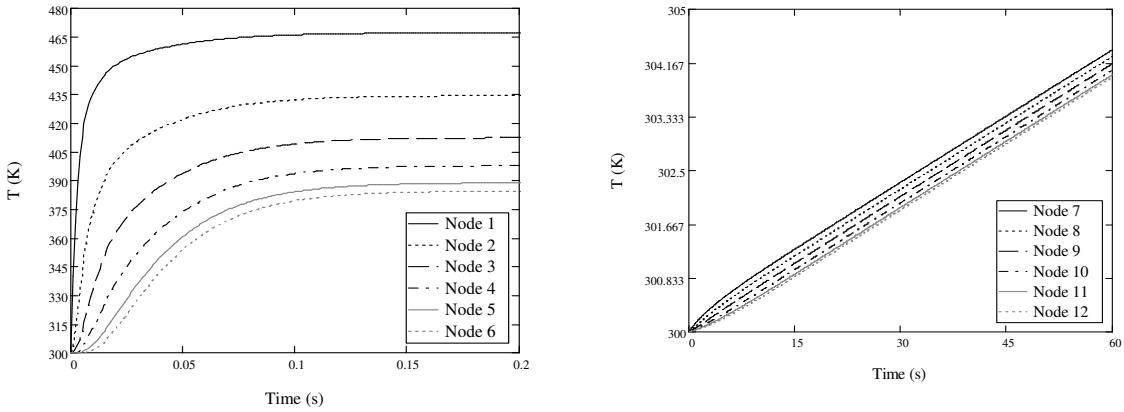

(a) **(b)**

Figure 13. Cooling characteristics of the circular duct (m ̇_Air=0.36kg/h): a) Air, b) Aluminum substrate

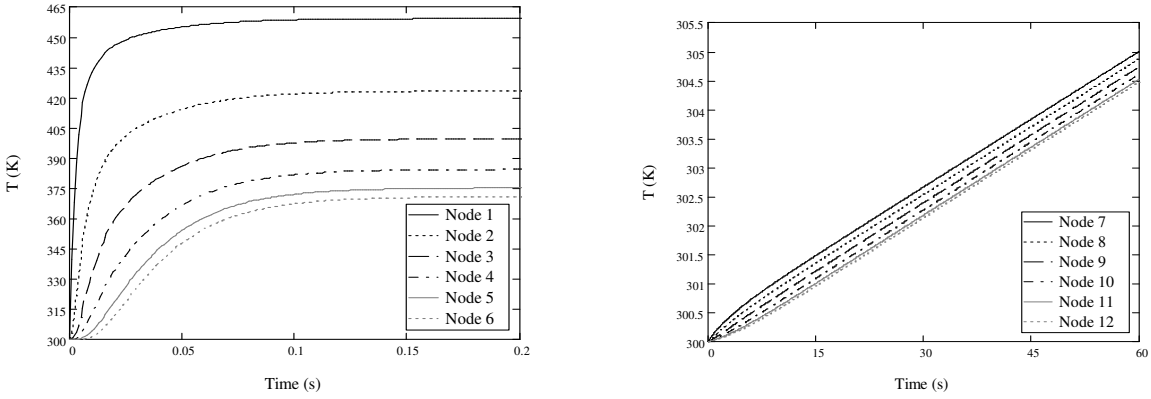

(a) **(b)**

Figure 14. Cooling characteristics of the square duct (m ̇_Air=0.36kg/h): a) Air, b) Aluminum substrate.

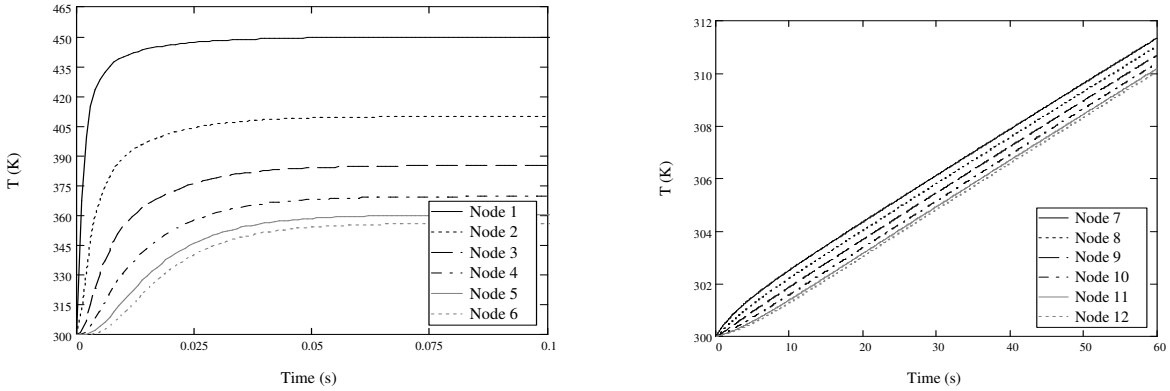

(a) **(b)**

Figure 15. Cooling characteristics of the triangular channel ($\dot{m}_{Air} = 0.72kg/h$): a) Air, b) Aluminum substrate

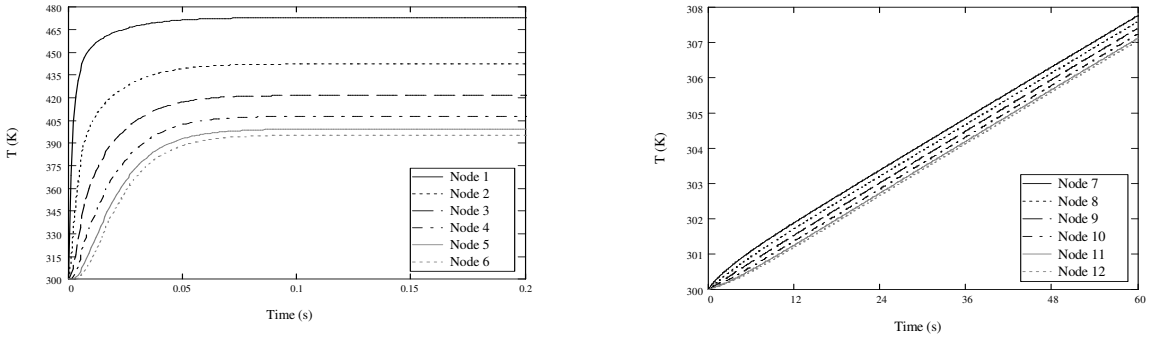

(a) **(b)**

Figure 16. Cooling characteristics of the rectangular duct (m ̇_Air=0.72kg/h): a) Air, b) Aluminum substrate.

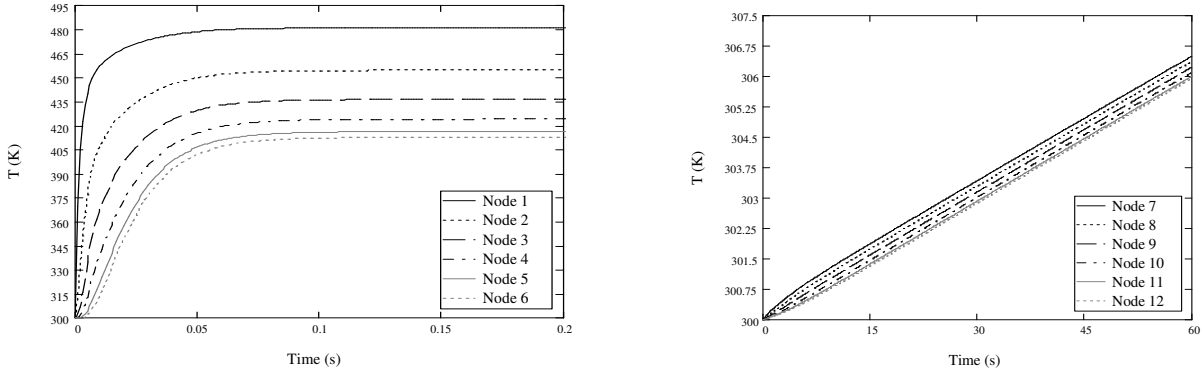

(a) **(b)**

Figure 17. Cooling characteristics of the circular duct ($\dot{m}_{Air} = 0.72kg/h$): a) Air, b) Aluminum substrate.

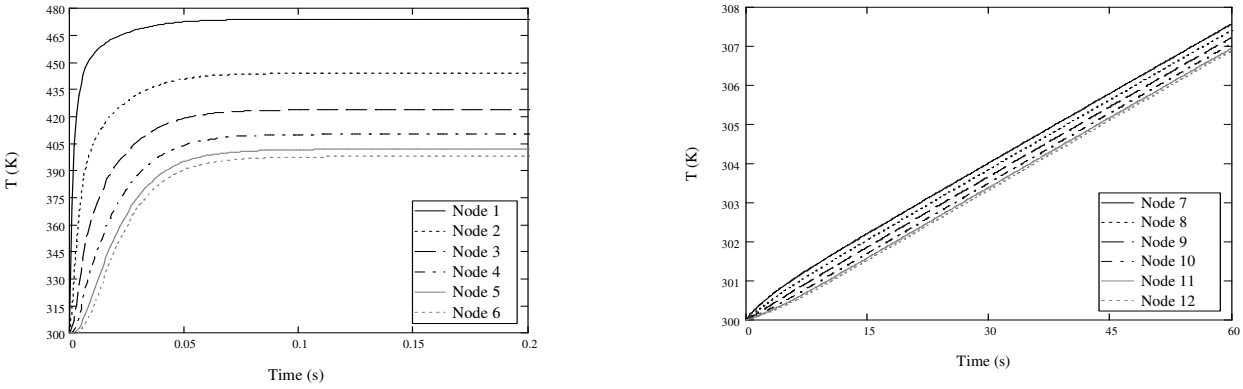

(a) **(b)**

Figure 18. Cooling characteristics of the square duct ($\dot{m}_{Air} = 0.72kg/h$): a) Air, b) Aluminum substrate.

4.2. Pump Power Requirement

Required pump power of each duct was calculated (See Table 3). Individual effects of f, D_h, and T_m (a measure of the extent of heat transfer) were identified on the calculated Δp values. Triangular duct was the most favorable in terms of this requirement.

Table 3 Δp values calculated of the ducts

cross-section	$f \cdot Re_{Dh}(T_m)$[1] $[-]$	Δp[2] $[Pa]$	v_m $[m/s]$
	$\dot{m}_{Air} = 0.036kg/h$		
circular	64.0	0.305	0.314
square	57.0	0.27	0.314
rectangular	59.4	0.281	0.313
triangular	53.0	0.249	0.312
	$\dot{m}_{Air} = 0.18kg/h$		
circular	64.0	1.699	1.641
square	57.0	1.473	1.622
rectangular	59.4	1.532	1.621
triangular	53.0	1.293	1.585
	$\dot{m}_{Air} = 0.36kg/h$		
circular	64.0	3.591	3.363
square	57.0	3.111	3.321
rectangular	59.4	3.228	3.315
triangular	53.0	2.683	3.217
	$\dot{m}_{Air} = 0.72kg/h$		
circular	64.0	7.578	6.905
square	57.0	6.561	6.809
rectangular	59.4	6.805	6.793
triangular	53.0	5.613	6.555

[1] For the fully-developed laminar flow (Bergman *et al.*, 2011). [2] $\Delta p = \frac{2 \cdot f \cdot \dot{m}_{Air}(T_m) \cdot L \cdot v_m}{\pi \cdot D_h^3} = f \cdot \frac{L}{D_h} \cdot \rho_{Air}(T_m) \cdot \frac{v_m^2}{2}$. $\rho_{Air}(T_m)$ was calculated at $T_m = (T_{in} + T_6)/2$.

5. CONCLUSIONS

Air cooling characteristics were studied on the triangular, rectangular, circular, and square cross-section ducts. In terms of the extent of air cooling and pump power requirement, triangular cross-section duct was the most favorable over other duct types. Rectangular and square cross-section ducts followed next. The thermal analysis results were given under the laminar flow condition of air. 1-D duct flow was analyzed. The results were presented on the relatively short combined entry regions of the ducts.

The analysis performed in this paper focused on the cooling effectiveness of the high-temperature air. The results can be used to choose the appropriate duct type in the design phase before the manufacture. No generalizations have been made for other fluids. No generalizations have been made for other flow conditions. The same ducts can be analyzed with the same set of equations to study the cooling of the other high-temperature fluids.

NOMENCLATURE

Letters

A area (m^2)
C thermal mass, $m \cdot c_p$, $(J \cdot K^{-1})$
c specific heat $(J \cdot kg^{-1} \cdot K^{-1})$
D diameter (m)
f friction factor $(-)$
Gz Graetz number, $D_h \cdot x^{-1} \cdot Re_{Dh} \cdot Pr$
H height (m)
h convective heat transfer coefficient $(W \cdot m^{-2} \cdot K^{-1})$
k thermal conductivity $(W \cdot m^{-1} \cdot K^{-1})$
L length (m)
m mass (kg)
Nu Nusselt number, $h \cdot D_h \cdot k^{-1}$
n number of nodes $(-)$
P wetted perimeter (m)
Pr Prandtl number, $\nu \cdot \alpha^{-1}$
p pressure (Pa)
Re Reynolds number, $v_m \cdot D_h \cdot \nu^{-1}$
r radius (m)
T temperature (K)
V volume (m^3)
v velocity $(m \cdot s^{-1})$
W width (m)
x x-coordinate (m)

Greeks

Δ finite
μ dynamic viscosity $(kg \cdot m^{-1} \cdot s^{-1})$
ρ density $(kg \cdot m^{-3})$

Subscripts

Air	air
Al	aluminum
b	bulk
c	cross-section
D_h	hydraulic diameter
d	duct
f	flow
fd, h	fully-developed (hydrodynamic)
fd, t	fully-developed (thermal)
h	hydraulic
in	inlet
lat	lateral
m	mean (average)
o	inner
out	outlet
p	constant pressure (isobaric)
s	substrate
s	surface
x	local

Superscripts

+	non-dimensional quantity
′	calculated

Others

·	time-rate
−	average
∞	infinite

REFERENCES

1. Bergman, T.L., Lavine, A.S., Incropera, F.P., and Dewitt, D.P. (2011), Fundamentals of Heat and Mass Transfer,7thed., p. 539, p. 543, p. 553, p. 983, p. 995,John Wiley & Sons, Inc., New York, NY.
2. Chen, Y., Zhang, C., Shi, M., and Wu, J.(2009), "Three-dimensional numerical simulation of heat and fluid flow in noncircular microchannelheat sinks", International Communications in Heat and Mass Transfer, Vol. 36 No. 9, pp. 917-920.
3. Kays, W.M. and Crawford, M.E.(1993), Convective Heat and Mass Transfer, 3rd ed., p. 151, p. 346, McGraw-Hill, Inc., New York, NY.
4. Kong, K.S. and Ooi, K.T.(2013), "A numerical and experimental investigation on microscale heat transfer effect in the combined entry region in macro geometries",International Journal of Thermal Sciences, Vol. 68, pp. 8-19.
5. Mohammed, H.A.and Salman, Y.K.(2007), "Free and forced convection heat transfer in the thermal entry region for laminar flow ınside a circular cylinder horizontally oriented", Energy Conversion and Management, Vol. 48 No. 7, pp. 2185-2195.

6. Nguyen, T.V.(1993), "Incremental heat transfer number in the entry region of circular tubes", International Journal of Heat and Mass Transfer, Vol. 36No. 14, pp. 3659-3662.
7. Sarma, P.K., Kishore, P.S., Subrahmanyam, T., and Rao, V.D.(2004), "A novel method to determine laminar convective heat transfer in the entry region of a tube", International Journal of Thermal Sciences, Vol. 43 No. 6, pp. 555-559.
8. Sieder, E.N. and Tate, G.E.(1936), "Heat transfer and pressure drop of liquids in tubes", Industrial & Engineering Chemistry, Vol. 28 No. 12, pp. 1429-1435.